Composites Part B 245 (2022) 110209

Contents lists available at ScienceDirect

Composites Part B

journal homepage: www.elsevier.com/locate/composites

Investigating the transfer of toughness from rubber modified bulk epoxy polymers to syntactic foams

Sammy He [a], Declan Carolan [a,b], Alexander Fergusson [a,b], Ambrose C. Taylor [a,*]

[a] Department of Mechanical Engineering, Imperial College London, South Kensington Campus, London SW7 2AZ, UK
[b] FAC Technology, 53 Lydden Grove, Wandsworth, London SW18 4LW, UK

ARTICLE INFO

Keywords:
Syntactic foams
Toughening
Fracture toughness
Lightweighting

ABSTRACT

Syntactic foams are lightweight, high specific strength materials used in the aerospace and naval industries. Their utility is limited by their brittleness. The epoxy polymer matrix in an epoxy/hollow glass microsphere (GMS) syntactic foam was modified using carboxyl-terminated butadiene-acrylonitrile (CTBN) rubber with the aim to increase fracture toughness. The microstructure and fracture properties were investigated, and compared to CTBN modified bulk epoxy polymers. The formation of complex CTBN microstructures was responsible for the increase in fracture energy, from 193 J/m^2 for the unmodified syntactic foam, to 296 J/m^2 at 12 wt% CTBN modification. However, this increase is much smaller than for the CTBN modification of bulk epoxy polymers, where an increase from 101 J/m^2 to 1112 J/m^2 was measured for the same CTBN concentration. There is little toughness transfer from the bulk epoxy polymers to the syntactic foams, attributable to small interstitial regions between the GMS, restricting plastic zone size. A statistical approach to the analytical modelling of fracture energy in the bulk epoxy polymers highlights the importance of considering the underlying distribution of rubber particle and void sizes. The increase in fracture energy achieved in this work can increase the overall usefulness of syntactic foams in structural applications.

1. Introduction

Syntactic foams are strong, lightweight composite materials comprising hollow particles in a matrix material. The most commonly used form of syntactic foam comprises hollow glass microspheres (GMS) in an epoxy polymer matrix, which is used in this work. Since the majority of the porosity of the syntactic foam is contained within the hollow spheres (with a very small amount due to manufacturing defects), the material exhibits desirable properties such as low density, high compressive strength and high specific strength compared to conventional foams, while also exhibiting low moisture absorption and low thermal and electrical conductivity [1,2]. Originally developed in the 1960s for buoyancy aid systems [3], recent research into syntactic foams has rapidly made them attractive for structural, weight-sensitive applications in the aerospace and marine industries [4].

In recent years, syntactic foams have gained popularity as core materials in sandwich composite structures [5–7], which are used in aircraft interior walls, ceilings, floors, and cargo pallets [8]. The uses of composites in aerospace and naval applications have continued to become more prevalent [9,10], as they allow for weight reductions without compromising load bearing capacity, thus improving fuel efficiency. Whilst still lightweight, syntactic foams provide superior mechanical properties compared to commonly used core materials, such as open cell foams, honeycomb, or corrugated structures [5,8,11]. The high level of tailorability of the density and mechanical properties of the syntactic foam is a major advantage responsible for this increased popularity, since the volume fraction [12], diameter [13,14], and wall thickness [15,16] of the hollow glass microspheres are parameters that can be independently varied to meet the application requirements.

Despite these advantages, the applications of syntactic foams are limited due to their brittle nature, since they are based on a highly crosslinked thermosetting polymer. Most studies in the literature have explored the introduction of reinforcing particles, such as nanoclay [17,18], graphene platelets [19,20], carbon nanofibres [21,22], and various high aspect ratio microfibres [23–25] to improve the mechanical and fracture properties of syntactic foams, each with varying degrees of success (ranging from 25%–180% increases relative to the base material). However, the direct modification of the epoxy matrix to achieve greater fracture toughness has been relatively unexplored. For bulk epoxy polymers which are used in structural applications, toughening is required to resist the growth of defects and subsequent failure, which can be achieved through the addition of a second phase into the material. The most successful and commonly used approach has been

* Corresponding author.
E-mail address: a.c.taylor@imperial.ac.uk (A.C. Taylor).

https://doi.org/10.1016/j.compositesb.2022.110209
Received 11 May 2022; Received in revised form 6 July 2022; Accepted 10 August 2022
Available online 15 August 2022

the incorporation of rubbery particles. Reactive liquid rubbers, such as carboxyl-terminated butadiene-acrylonitrile (CTBN), were first utilised in the 1970s by Sultan and McGarry [26]. These rubbers are usually pre-dissolved in the epoxy resin as an adduct, and phase separate during the curing process to form micron-sized rubber particles. The growth evolution of the rubbery phase in the epoxy can be described by the Cahn–Hilliard equation [27,28], which is dependent on the rubber concentration and mobility of the mixture, and controls the size and morphology of the phase separated rubber particles. There have been many studies which report significant increases in fracture toughness with the addition of CTBN in the epoxy polymer [29], and it is generally accepted that shear band yielding, rubber particle cavitation and subsequent matrix void growth are the main toughening mechanisms responsible, and the analytical modelling of these toughening mechanisms has been well-established [30]. However, whether these increases in toughness can transfer to syntactic foams when CTBN modified epoxy is used as the matrix is currently not well understood.

To overcome the brittleness of syntactic foams, this study investigates the effect of using CTBN rubber as a toughening modifier in bulk epoxy polymers, and in the epoxy matrix of syntactic foams. The morphologies of the CTBN rubber particles are compared for the two material types, and the differences are explained in terms of phase separation and preferential surface adsorption. The fracture properties were also measured and compared, particularly to assess how effectively the increased fracture properties were transferred from the bulk material to the syntactic foam. Scanning electron microscopy was then used to identify the toughening mechanisms involved, and the analytical modelling of these toughening mechanisms is discussed. In the analytical modelling of fracture energy, a statistical approach that considers the underlying size distribution of particle and void diameters was used, and this was compared to the more simplistic mean-value approach that has been conventionally used in the literature [31]. The results from the analytical modelling using these two approaches are compared to the experimental values to assess their agreement. This work highlights the capabilities and shortcomings of using rubber toughening approaches for toughening highly filled particulate composites such as syntactic foam.

2. Experimental

2.1. Materials and manufacturing

Plates of bulk epoxy polymer and syntactic foam were manufactured such that comparison of the morphology, mechanical and fracture properties, and toughening mechanisms of the two materials could be made. The epoxy resin was a standard diglycidyl ether of bisphenol-A (DGEBA), 'Araldite LY556', with an epoxide equivalent weight (EEW) of 185 g/eq. The curing agent was a methyltetrahydrophthalic anhydride, 'Aradur HY917', with an anhydride equivalent weight (AHEW) of 166 g/eq. An accelerator in the form of a heterocyclic amine catalyst, 1-methylimidazole, 'Accelerator DY070', was also used. All epoxy components were supplied by Huntsman, UK. The epoxy, curing agent, and accelerator were used at a stoichiometric ratio of 100:90:1, respectively.

Carboxyl-terminated butadiene-acrylonitrile (CTBN) reactive liquid rubber was used as a toughening agent for the epoxy polymer. The CTBN rubber was supplied as an adduct, pre-reacted and dissolved in DGEBA resin as 'Albipox 1000', by Evonik, Germany. This has an EEW of 330 g/eq [32], and has 40 weight percentage (wt%) CTBN rubber content. To prepare the bulk epoxy material, the required concentration of CTBN rubber was obtained by diluting the masterbatch with additional DGEBA, 'Araldite LY556'. The mixture was then heated in an oven to 60 °C and stirred using a mechanical stirrer for at least 10 min at 200 rpm until no mixing lines were visible, indicating homogeneity. A stoichiometric amount of the anhydride curing agent and accelerator were added, and stirred thoroughly for another 10 min. The mixture was then degassed in a vacuum oven at 60 °C and −1 atm for at least 15 min, until no additional air bubbles were formed. This was then poured into release-coated (using 'Loctite Frekote 770NC' from Henkel, UK) steel vertical moulds of thicknesses 3 mm and 6 mm. The epoxy was cured at in an oven at 80 °C for 4 h, followed by a post-cure at 140 °C for 8 h, as recommended by Huntsman [33]. Bulk epoxy polymer plates with up to 12 wt% CTBN were manufactured. In the literature, 9 wt% of CTBN is typically the optimum concentration in terms of achieving the greatest fracture toughness [34–36].

Table 1
Volume fraction of CTBN for the CTBN modified bulk epoxy polymers.

CTBN concentration (wt%)	CTBN volume fraction V_p
Unmodified	0
3	0.037
6	0.074
9	0.110
12	0.146

The density of the CTBN rubber was taken from the literature [37] as 948 kg/m^3, and the density of the epoxy was measured to be 1190 kg/m^3 [23], so that the volume fraction of the CTBN rubber, V_p, which is used in the analytical modelling of fracture energy, can be determined. The volume fractions are shown in Table 1 for each of the formulations.

Borosilicate hollow glass microspheres (GMS) of type 'S38' from 3M, UK, were used to manufacture the syntactic foams. These microspheres have a mean diameter of 40 μm, a mean wall thickness of 1.28 μm with no porosity, a true density of 380 kg/m^3, a crush strength of 27.6 MPa (for 90% survival), and no surface treatment [38]. The syntactic foams were manufactured so that the GMS are densely packed, up to a packing factor of approximately 60%, according to the product data sheet [38]. This is to maximise the hollow content provided by the GMS, thus reducing density and weight which is desirable in the weight-sensitive applications in which syntactic foams are commonly used. This packing factor was confirmed in a previous study [23], where a volume fraction of 60.7% was measured by performing volume fraction analysis on optical microscopy images of the syntactic foam cross-sections. The CTBN modified epoxy polymer matrix was prepared using the same method described above for the bulk material. Epoxy polymer matrices with up to 12 wt% CTBN rubber were used. The GMS are embedded into the epoxy matrix and the plates of syntactic foam were manufactured in a mould, and were subject to the same curing cycle as the bulk epoxy polymer. The plates produced were then milled to a thickness of 8 mm using a TM-2 CNC machine from Haas, UK.

2.2. Thermal testing

2.2.1. Dynamic mechanical analysis

The glass transition temperature, T_g, values of the bulk epoxy polymers and syntactic foams were determined using dynamic mechanical analysis (DMA) using a 'Q800 DMA' from TA Instruments, UK. Specimens of dimensions 60 × 10 × 3 mm^3 were tested in double cantilever mode, in accordance with the ASTM D5418-15 [39] test standard. The tests were conducted over a temperature range of −100 to 200 °C, at a heating rate of 2 °C/min. The samples were loaded sinusoidally with a strain amplitude of 0.01% at a fixed frequency of 1 Hz. The storage modulus, E', loss modulus, E'', and the loss factor, $\tan\delta$, were recorded against temperature. The glass transition temperature was determined at the peak value of $\tan\delta$. At least one sample from each bulk epoxy and syntactic foam formulation was tested.

2.3. Bulk mechanical testing

2.3.1. Plane strain compression

Plane strain compression (PSC) tests were performed on the bulk epoxy polymers to determine the plane strain compressive yield stress,

$\sigma_{y,psc}$, and the true compressive failure strain, γ_f, as described by Williams and Ford [40]. Polished specimens of dimensions 40 × 40 × 3 mm^3 were first lubricated with 'High Temperature Grease' from Castrol, UK, and were compressed between two 12 mm wide parallel dies using an Instron 5585H universal testing machine fitted with a 250 kN load cell at a displacement rate of 0.1 mm/min. The results from the tests were then corrected for the machine and rig compliances, which were determined by conducting a test without a specimen. Since polishing of the PSC samples is very time-consuming, at least two specimens were tested for each formulation. However, the repeatability of these tests has been found to be very good in the literature, and two is the typical number of specimens used for plane strain compression testing [41–43].

The plane strain compressive stress, σ_{psc}, was calculated by dividing the compressive load, P, by the width of the dies, W, and the length of the sample, L:

$$\sigma_{psc} = \frac{P}{WL} \tag{1}$$

The true compressive strain, γ, can be calculated using:

$$\gamma = \frac{2}{\sqrt{3}} \ln \frac{h}{h_0} \tag{2}$$

where h and h_0 are the deformed and initial thicknesses of the sample, respectively.

2.3.2. Single edge notch bending

The fracture toughness, K_{IC}, and fracture energy, G_{IC}, of the bulk epoxy polymers and syntactic foams were obtained by conducting single edge notch bending (SENB) tests, in accordance with the ISO 13586 [44] test standard. For the bulk epoxy polymers, specimens of dimensions 60 × 12 × 6 mm^3 were cut, and a V-notch of angle 60° was machined at the mid-length to a depth of 4 mm using a horizontal mill. For the syntactic foams, specimens of dimensions 80 × 16 × 8 mm^3 were cut, and a V-notch of 5.3 mm depth was milled at the mid-length. A liquid nitrogen cooled razor blade was then carefully tapped into the V-notch to produce a sharp pre-crack before testing. The syntactic foam specimens were larger to ensure plane strain conditions ahead of the crack tip during the SENB tests in order to satisfy the size criteria specified in the test standard [44]. At least ten valid tests were performed for each bulk epoxy polymer and syntactic foam formulation.

2.4. Imaging studies

2.4.1. Atomic force microscopy

The morphology of the bulk epoxy polymers was determined using atomic force microscopy (AFM). A scanning probe microscope, 'Multi-Mode 8', equipped with an 'E' scanner and controlled by a 'NanoScope IV' controller (from Veeco, USA) was used. Flat and smooth surfaces were cut on the samples using a ultramicrotome, 'PowerTome XL', from RMC Products, USA. The ultramicrotome was operated at room temperature. Phase images of resolution 512 × 512 pixels at scan sizes of 20 × 20 μm^2 and 50 × 50 μm^2 were obtained using silicon probes, operated in tapping mode at a scan speed of 1 Hz. Soft material will appear darker in the phase images so that the CTBN rubber can be readily identified.

2.4.2. Scanning electron microscopy

The fracture surfaces of the SENB samples of the bulk epoxy polymers and syntactic foams were observed using scanning electron microscopy (SEM) to identify the toughening mechanisms. A Hitachi 'S-3400N' scanning electron microscope was used. The samples were mounted on aluminium stubs using electrically-conductive pressure-sensitive tape and sputter coated with a 10 nm thick layer of gold to minimise charging. A working distance of 10 mm and an accelerating voltage of 10 kV were used.

2.4.3. Optical microscopy

To observe the shear bands in the plane strain compression samples, and to confirm the presence of the shear band yielding toughening mechanism in the CTBN modified epoxy polymers, a specimen from each formulation was loaded to the strain softening region in the PSC tests. A thin section was cut from each of the samples in the middle of the compressed region using a 'Brillant 220' cut-off machine from ATM, Germany, equipped with a diamond blade. Each section was mounted onto a glass microscopy slide using an optically transparent adhesive, 'Araldite 2020', from Huntsman, UK, and then ground and polished to a nominal thickness of 100 μm. An optical microscope, 'AxioScope.A1', from Carl Zeiss, Germany, was used in transmission mode to obtain optical micrographs of the polished sections. The sample was placed between crossed polarisers and imaged using white light.

3. Results & discussion

3.1. Glass transition temperature

The glass transition temperatures of the CTBN modified epoxies were measured using dynamic mechanical analysis (DMA). The $\tan\delta$ curves are shown in Fig. 1(a), and the T_g of the epoxy polymer is extracted from the main high-temperature peak. As well as the main peak, a much shorter but still distinct peak emerges at −48 °C, which is the glass transition temperature of the CTBN rubber, see Fig. 1(b) which focuses on the low temperature region. This peak becomes more apparent at higher CTBN concentrations. This glass transition temperature of the CTBN is consistent with other works studying CTBN rubber modified epoxies, e.g. [36,45–47].

The measured T_g for each of the formulations is summarised in Table 2. The unmodified epoxy has a T_g of 151 °C, which is in agreement with the data sheet for this epoxy system [33]. Adding 3 wt% CTBN did not change T_g, indicating that the CTBN rubber exhibited complete phase separation during cure. However, T_g decreased to 146 °C for 6 and 9 wt% concentrations of CTBN, and decreased further to 137 °C for 12 wt% CTBN. This corresponds to a drop of 4 °C and 14 °C, respectively, compared to the unmodified epoxy polymer. This indicates that some of the rubber remains dissolved in the epoxy, and has thus caused a plasticising effect. The amount of CTBN that did not phase separate can be estimated using the Fox equation [48]:

$$\frac{1}{T_g} = \frac{W_e}{T_{g,e}} + \frac{W_{\mathrm{CTBN}}}{T_{g,\mathrm{CTBN}}} \tag{3}$$

where W is the weight fraction, and the subscripts e and CTBN represent the epoxy and CTBN rubber, respectively. Using $T_{g,e}$ = 151 °C and $T_{g,\mathrm{CTBN}}$ = −48 °C in the Fox equation, the decreases of 4 °C and 14 °C correspond to an estimated 1.1 wt% and 4.0 wt% of CTBN rubber remaining dissolved for the 9 wt% and 12 wt% CTBN formulations, respectively.

The CTBN modified syntactic foams follow the same trends, however the height of the peak in $\tan\delta$ was lower than for the bulk epoxy polymers over the whole temperature range, due to the reduced volume of epoxy polymer and increased stiffness caused by the presence of GMS. The secondary peak at −48 °C, representing the T_g of the CTBN rubber, was also observed for the syntactic foams. The T_g of the syntactic foams did not differ significantly from that of the bulk epoxy polymers, see Table 2, which indicates that the hollow glass microspheres did not affect the extent of phase separation of CTBN. The amount of CTBN remaining dissolved in the syntactic foam was similar to that in the bulk epoxy polymers. Thus, the presence of the microspheres did not significantly affect the curing of the epoxy.

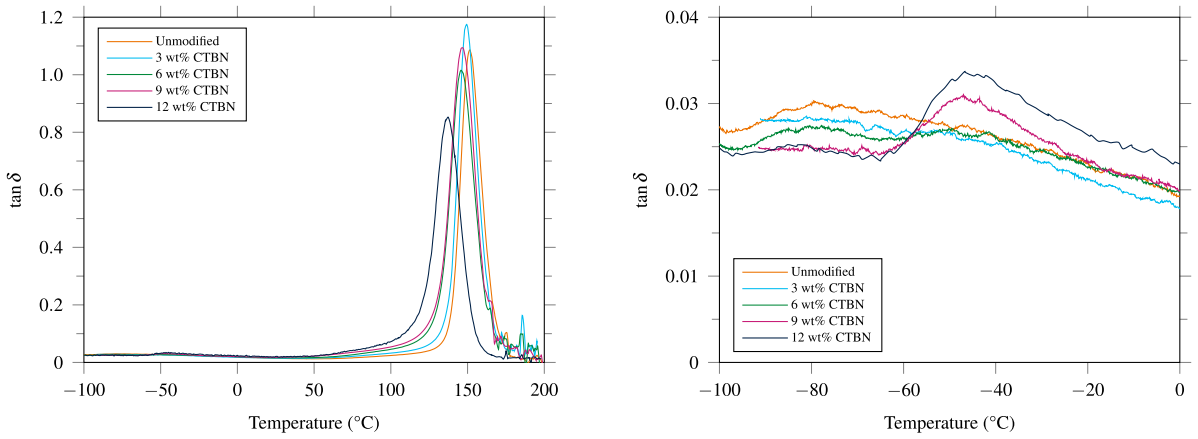

Fig. 1. **(a)** Tan δ versus temperature for the CTBN rubber modified bulk epoxy polymers. **(b)** Same as **(a)**, focusing on the low-temperature region.

Table 2
Glass transition temperatures, T_g, of CTBN modified bulk epoxy polymer and syntactic foam, and dissolved CTBN wt% calculated using the Fox equation [48]. Temperature values have a standard error of ±1 °C.

CTBN concentration	Bulk epoxy polymer		Syntactic foam	
(wt%)	T_g (°C)	Dissolved CTBN (wt%)	T_g (°C)	Dissolved CTBN (wt%)
Unmodified	151	–	153	–
3	149	0.7	150	0.5
6	147	1.1	148	0.9
9	147	1.1	148	1.0
12	137	4.0	136	4.1

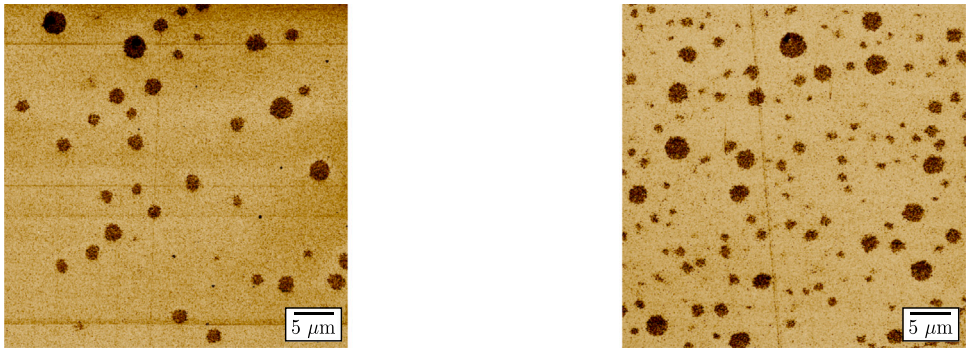

Fig. 2. AFM phase micrographs of CTBN rubber modified bulk epoxy polymers.

3.2. Microstructure

3.2.1. Bulk epoxy polymer

The morphology of the CTBN modified bulk epoxy polymers was determined using atomic force microscopy (AFM), and selected phase micrographs are shown in Fig. 2. The CTBN rubber particles are identified as dark regions in the phase images since they have a much lower stiffness compared to the epoxy. These micrographs are an illustrative, typical representation of the CTBN particles before fracture, hence the initial particle radius can be measured. This is then compared to the radius of the voids on the fracture surface, which will indicate whether the plastic void growth toughening mechanism has occurred, as discussed later in Section 3.5.1.

The dark circular features on the AFM images show that the CTBN rubber has phase separated into well-dispersed spherical particles within the bulk epoxy. By inspection of the AFM micrographs, the distribution of rubber particle sizes is assumed to be the same for all CTBN concentrations. This has been observed by Kinloch and Hunston [49], where no significant differences in mean particle radius were measured in a similar range of CTBN concentrations. Therefore, measurements using the 9 wt% CTBN modified epoxy were used to represent all CTBN concentrations.

The flat and smooth surface required for AFM was cut using microtoming, and it is impossible that all of the rubber particles would be sectioned at their equators. An uncorrected size distribution will therefore reflect where the particles are cut (e.g. near the poles or at the equators) as well as the variation in particle radius. This was corrected using stereological methods, which are outlined in [50]. The radii of the CTBN particles were measured and a mean value of 0.87 ± 0.38 μm was obtained. A normalised histogram, corresponding to 420 radius measurements, is shown in Fig. 3. The histogram appears to follow a log-normal distribution, which was expected since they are often found to closely approximate the size distribution of many types of nanomodifiers [31,51]. A log-normal probability density function (PDF)

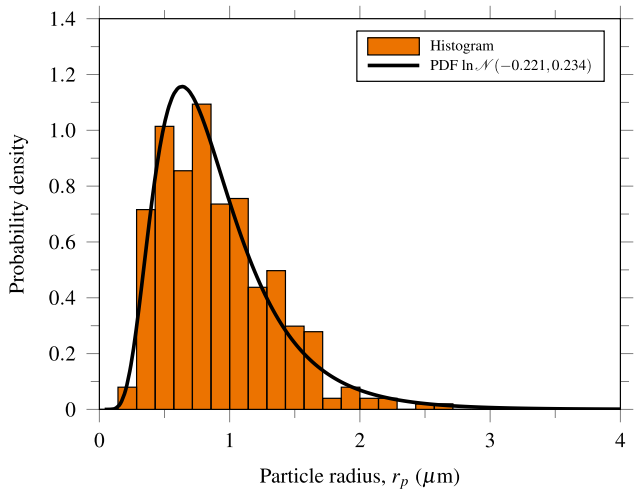

Fig. 3. Probability density distribution of particle radii from AFM micrographs of 9 wt% CTBN rubber modified epoxy polymer.

is overlaid on the histogram, and fits well to the experimental data. The PDF uses the statistical parameters following the notation:

$$r_p \sim \ln \mathcal{N}\left(\mu, \sigma^2\right) \tag{4}$$

where r_p is the radius of the particle, and the statistical parameters μ and σ are the mean and standard deviation of the logarithmic radius values, respectively. The mean logarithmic radius, μ, is −0.221, and the standard deviation of the logarithmic radius, σ, is 0.234.

Many studies on rubber modified epoxies do not consider the underlying distribution of particle sizes and have conventionally used only the mean value of particle radius in the modelling of fracture energy. Although the mean particle radius was measured to be 0.87 μm in this study, the PDF shows that the modal radius, which is therefore the most statistically probable, is smaller at 0.63 μm. The significance of this will be discussed below.

3.2.2. Syntactic foam

It was not possible to use atomic force microscopy to determine the morphology of the CTBN rubber in the syntactic foam, due to the large size of the GMS relative to the scanning area of the AFM. The morphology of the CTBN rubber in the epoxy matrix of the syntactic foam was inferred from SEM images of the fracture surfaces, which are shown in Fig. 4. The images confirm that CTBN rubber was present in the interstitial spaces between the microspheres.

For the syntactic foams with 3 wt% CTBN modified epoxy, circular features such as those seen in Fig. 4(a) suggest that the CTBN has phase separated into spherical particles. When the CTBN concentration increases to 6 wt%, some particles remain spherical, while some particles begin to elongate along the surface of the glass microspheres. The elongation increases with the 9 wt% CTBN modified syntactic foam, where rubber particles that have a characteristic length of up to 10 μm, such as those in Fig. 4(c), can be seen. These indicate that co-continuous structures of CTBN were formed. When the CTBN concentration is further increased to 12 wt%, lamellar structures of alternating CTBN and epoxy layers are seen, see Fig. 4(d). Phase inversion is also evident, where voids left by epoxy particles within rubber-rich regions of up to 10 μm in diameter are observed, see Fig. 5. These voids have an average diameter of 2 μm and are much smaller than the GMS, so it can be inferred they were left by epoxy particles. Clearly, the presence of GMS has caused the CTBN to phase separate into a complex microstructure that is radically different to that seen for the bulk epoxy polymer, where all of the CTBN particles were spherical for all of the volume fractions of CTBN investigated.

3.2.3. Phase separation

The presence of co-continuous structures of rubber in the epoxy matrix of the syntactic foam indicates that the CTBN phase separated via the spinodal decomposition mechanism [52]. This is opposed to the nucleation and growth mechanism where only spherical morphologies are possible [53], although spinodal decomposition can also form spherical particles. Structures that are formed during phase separation are fixed in place as the epoxy reaches gelation. This is due to the viscosity of the resin increasing as crosslinks are established, and the molecular mobility is greatly restricted.

In a mixture containing a primary and secondary phase, the process that governs spinodal decomposition was proposed by Cahn and Hilliard [27], and is dependent on the mobility of the mixture, and the concentration of the secondary phase. At low concentration values of the secondary phase, spherical particle morphologies were formed, while at larger concentrations, co-continuous structures are promoted [31]. This mirrors what was seen in the syntactic foams; spherical particles at 3 wt% CTBN, and co-continuous structures at 9 wt% and above. However, this does not occur for the bulk epoxy polymers as only spherical particles were observed. The transition from spherical to co-continuous structures in bulk epoxy polymers has been observed to occur at much higher concentrations (about 25 wt%) [54,55]. The difference in CTBN morphologies between the bulk epoxy polymer and syntactic foam was therefore compelling.

By observation of the SEM micrographs in Fig. 4, the CTBN particles appear to elongate along the geometry of the GMS, and are also up to an order of magnitude larger than the CTBN particles in the bulk epoxy. This observation is similar to work by Wiltzius and Cumming [56,57], who studied the influence of a quartz wall on the spinodal decomposition of a polyisoprene and poly(ethylene-propylene) blend. Using light-scattering, they observed that phase separated domains in the bulk away from the wall grew as an exponent of time that is proportional to $t^{1/3}$, which is typical with diffusion-driven dynamics (phase separation is a diffusion process [27]). However, the growth of the domains that were near the wall accelerated greatly, proportional to $t^{3/2}$, and these domains were also growing parallel to the surface. This behaviour could not be explained by diffusion- or interface-driven dynamics.

The authors attributed this behaviour to a wetting effect caused by one of the phases showing preferential adsorption to the quartz surface [57]. Adsorption is certainly present for the CTBN modified syntactic foams in this study. Epoxy molecules are preferentially adsorbed onto the surfaces of the GMS due to strong polar attractions between hydroxyl groups present on the epoxy molecules and the glass surfaces [58,59]. This is supported by the SEM images, where the GMS appear to be only coated with epoxy and never CTBN, even at high CTBN concentrations. This is highlighted clearly in Fig. 5 where the epoxy and CTBN phases are colourised in orange and dark blue, respectively. The epoxy therefore acts as the wetting component to the GMS surfaces.

Troian [60] developed this theory and proposed a mechanism for the increase in domain growth near a surface, as shown schematically in Fig. 6. When the wetting component adheres to the wall, the diffusive growth of the non-wetting component is slowed in the direction perpendicular to the wall, and will instead grow laterally to compensate (Fig. 6(b)). The wetting layer has therefore reduced the dimensionality of the diffusion process, as the 3D domains are now growing along a 2D surface.

By taking the radius of curvature of the non-wetting component at the surface to be much less than that in the bulk, Troian was able to prove that the diffusive growth due to the reduced dimensionality scales as $t^{1/2}$ (the full proof can be found in [60]). Further, the effect of particle coalescence (Fig. 6(c)) can accelerate this growth [61,62], to give the experimentally observed scaling of $t^{3/2}$ found by Wiltzius and Cumming [56,57].

For the case of the syntactic foam, it is difficult to determine the precise growth evolution of the CTBN particles since the gelation time

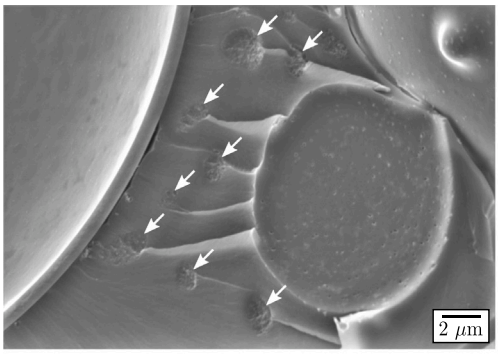

(a) 3 wt% CTBN

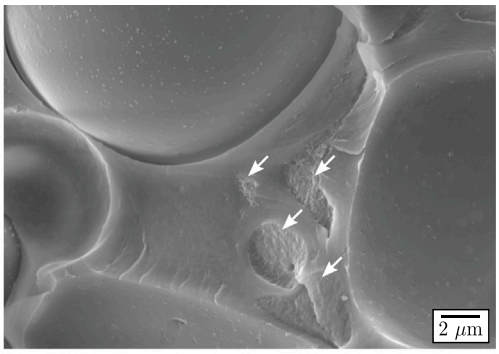

(b) 6 wt% CTBN

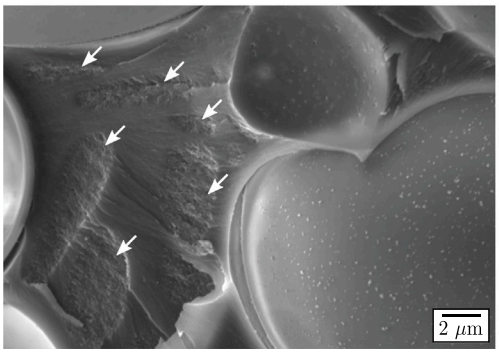

(c) 9 wt% CTBN

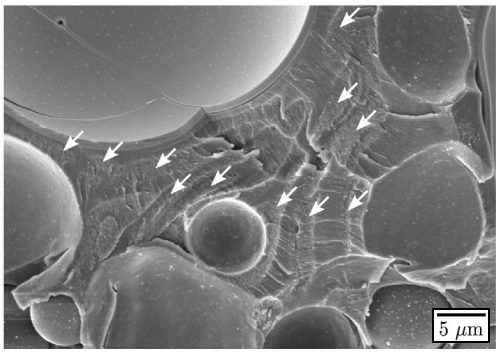

(d) 12 wt% CTBN

Fig. 4. Scanning electron micrographs of the fracture surfaces of CTBN rubber modified syntactic foams. Rubber particles are indicated by arrows. Crack propagation direction is from left to right.

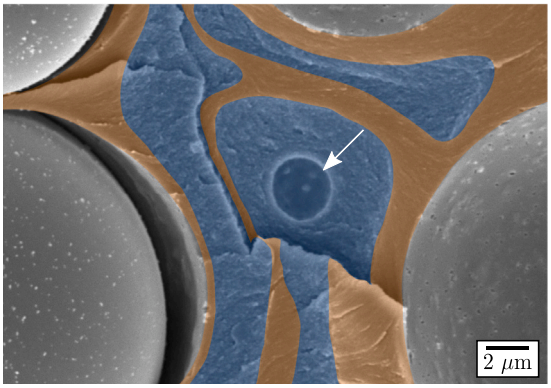

Fig. 5. Scanning electron micrograph of the fracture surface of 12 wt% CTBN modified syntactic foam. Epoxy and CTBN phases are colourised in orange and dark blue, respectively. A void within a rubber-rich phase left by an epoxy particle is indicated with an arrow. Crack propagation direction is from left to right. (For interpretation of the references to colour in this figure legend, the reader is referred to the web version of this article.)

of the epoxy is unknown. However, Wiltzius and Cumming observed the same $t^{1/3}$ and $t^{3/2}$ growth for the bulk and surface, respectively, regardless of quench depth [56,57]. An example growth evolution of the CTBN particles is presented in Fig. 7 for visual clarity. The radius of the CTBN particles is plotted against an arbitrary function of $t^{1/3}$ and $t^{3/2}$. After a given time before gelation (indicated by the dashed line in Fig. 7), the length scales are comparable to what was observed in the SEM images of the CTBN modified bulk epoxy and syntactic foam. The difference in CTBN particle morphology was thus determined to be due to reduced dimensionality and particle coalescence introduced by the presence of the glass microspheres.

3.3. Plane strain compression

Plane strain compression tests were performed on the unmodified epoxy polymer to determine the plane strain compressive yield stress, σ_{psc}, and the failure strain, γ_f. A typical stress–strain curve is shown in Fig. 8. The curve initially exhibits linear-elastic behaviour before reaching the yield point. This is followed by a strain softening region where the stress decreases with increasing strain. Strain softening is the result of inhomogeneous plastic deformation in the form of shear bands [63]. After the limit of strain softening, such deformation is stabilised and strain hardening occurs where the stress increases with increasing strain until the material finally fractures. The values for $\sigma_{y,psc}$ and γ_f were measured to be 122 ± 0.3 MPa and 0.87 ± 0.01, respectively, and these values will be used in modelling of the fracture energy, which is discussed in Section 3.6.

Epoxy polymers modified with CTBN rubber were also tested in plane strain compression as a qualitative comparison to the unmodified epoxy. The compressive behaviour of the CTBN modified epoxies shows that the degree of strain softening decreases with increasing CTBN concentration, with the 12 wt% CTBN epoxy showing no strain softening, see Fig. 8. This suggests that the formation of shear bands is being suppressed by the CTBN particles. This can be confirmed by using transmission optical microscopy. A sample from each formulation was loaded to within the strain softening region and then unloaded. The sample was then sectioned and polished to a nominal thickness of 100 μm. Transmission optical micrographs of the polished sections were taken using cross-polarised light, and are shown in Fig. 9.

The transmission optical micrograph for the unmodified epoxy in Fig. 9(a) clearly shows the macroscopic shear bands that were formed

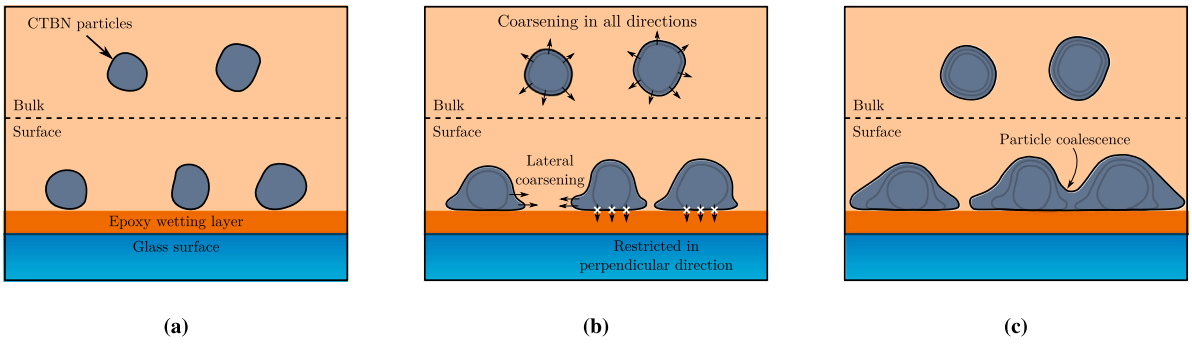

Fig. 6. Schematic diagram of CTBN particle growth in the bulk and near a surface during spinodal decomposition [60].

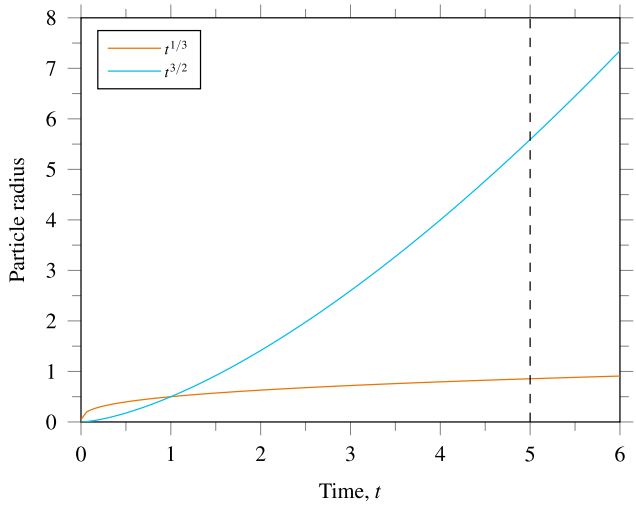

Fig. 7. Particle radius versus time where radius is an arbitrary function of $t^{1/3}$ (representing phase separation in a typical diffusion process) and $t^{3/2}$ (representing phase separation with reduced dimensionality and particle coalescence). The dashed line represents the time of gelation.

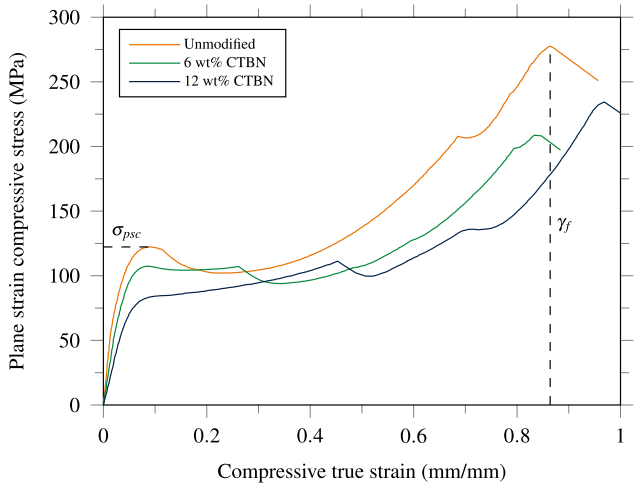

Fig. 8. Typical stress–strain curves for plane strain compression testing of CTBN modified epoxy polymers.

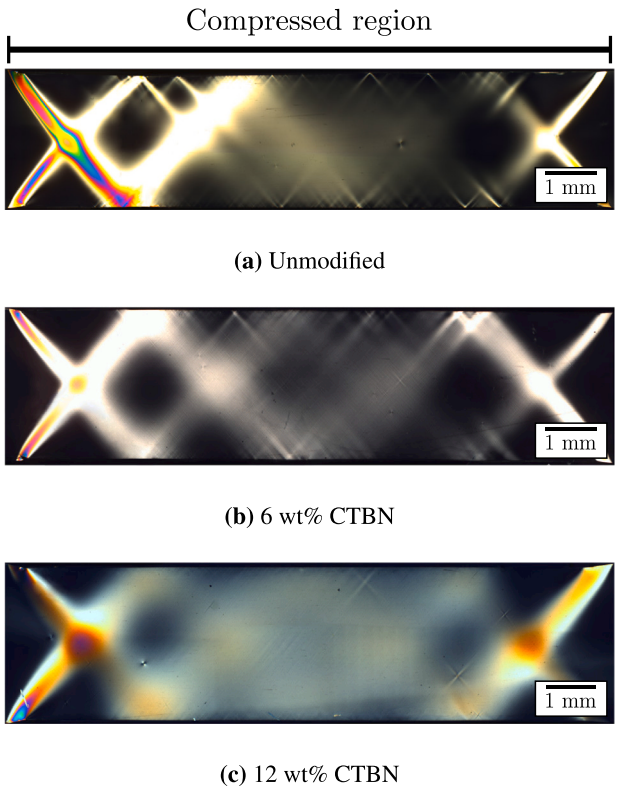

Fig. 9. Transmission optical microscopy images of plane strain compression specimens loaded to the strain softening region for (a) unmodified epoxy, (b) 6 wt% CTBN and (c) 12 wt% CTBN.

in the strain softening region as highly focused birefringence. Yielded regions of epoxy will have a different refractive index than the otherwise unrefractive non-yielded regions. Polarised light is therefore rotated after passing through the shear bands, which is why they appear bright under cross-polarised light. As the concentration of CTBN increases, the compressed region appears more diffuse, the intensity of the shear bands is decreased and the shear bands become less focused. This suggests that the CTBN particles have formed highly localised microscopic shear bands that initiate and terminate between adjacent particles due to the stress concentration effect around the particles. This was observed experimentally by Pearson and Yee [64] and also modelled using finite element analysis by Huang and Kinloch [65]. The formation of such highly localised microscopic shear bands between the rubber particles has thus suppressed the macroscopic inhomogeneous shear band deformation and also confirms the presence of the shear band yielding toughening mechanism.

3.4. Fracture properties

The fracture toughness, K_{IC}, and fracture energy, G_{IC}, of the CTBN modified bulk epoxy polymers and syntactic foams were determined using SENB tests. The results for the K_{IC} and G_{IC} values are shown in

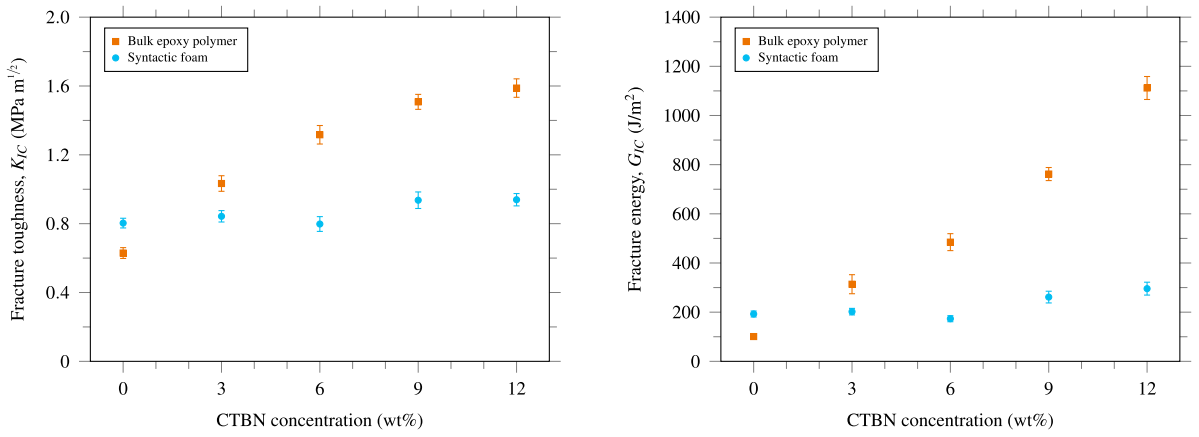

(a) Fracture toughness **(b)** Fracture energy

Fig. 10. Fracture properties of CTBN rubber modified bulk epoxy polymers and syntactic foams.

Fig. 10. The K_{IC} of the bulk epoxy polymer increases with increasing CTBN concentration, from 0.63 ± 0.03 MPa m$^{1/2}$ for the unmodified epoxy, to 1.59 ± 0.05 MPa m$^{1/2}$ for the 12 wt% concentration. The G_{IC} follows the same trend, from 101 ± 8 J/m^2 for the unmodified epoxy, to 1112 ± 47 J/m^2 for 12 wt% CTBN, corresponding to a 1000% improvement in fracture energy. This large increase in fracture performance is expected of rubber modified epoxies [29], due to the shear band yielding and plastic void growth toughening mechanisms [30], both of which are evident in this study. The shear band yielding was confirmed by the transmission optical micrographs of the plane strain compression specimens, as discussed in Section 3.3, while the plastic void growth mechanism can be confirmed by scanning electron microscopy of the fracture surfaces, which is discussed in Section 3.5.

For the syntactic foams, the unmodified foam had a K_{IC} of 0.80 ± 0.03 MPa m$^{1/2}$ and a G_{IC} of 193 ± 12 J/m^2. These values are larger than that of the unmodified bulk epoxy polymer, indicating that the GMS has provided some toughening. From a previous study [23], the main toughening mechanisms identified that were due to the GMS particles were crack deflection, debonding and plastic void growth. The triaxial stresses ahead of the crack tip cause the GMS particles within the plastic zone to debond from the epoxy matrix. This debonding relieves the stress triaxiality at the crack tip, hence allowing the matrix to deform via plastic void growth [66]. Gent [67] describes the debonding process as being dependent on the particle diameter, strength of the particle-to-matrix adhesion, and the modulus of the matrix. When the matrix of the syntactic foams was modified with CTBN, there was no change in K_{IC} and G_{IC} within experimental error at 3 and 6 wt% of CTBN. At higher concentrations, the fracture properties increased slightly, with K_{IC} of 0.94 ± 0.04 MPa m$^{1/2}$ and G_{IC} of 296 ± 26 J/m^2 achieved at 12 wt% CTBN. This corresponds to a 53% increase in fracture energy compared to the unmodified foam. While this improvement is comparable to those seen in the literature [17–22], it is significantly less than that seen for the bulk epoxy polymers.

The fracture energy values, and the change in fracture energy with respect to the unmodified material, ΔG_{IC}, are summarised in Table 3. Full transferability of toughness is achieved if ΔG_{IC} of the syntactic foam is equivalent to $0.4 \times \Delta G_{IC}$ of the bulk epoxy polymer, since 60% of the volume in the foam is occupied by GMS, leaving 40 vol% epoxy remaining. However, the ΔG_{IC} values are much smaller for all CTBN concentrations (see Table 3), therefore there is little transferability of toughness when CTBN modified epoxies are used as the matrix in syntactic foams. The reasons for this will be discussed below.

Table 3
Fracture energy, G_{IC}, and change in fracture energy, ΔG_{IC}, of CTBN modified bulk epoxy polymers and syntactic foams.

CTBN concentration	Bulk epoxy polymer (J/m^2)			Syntactic foam (J/m^2)	
(wt%)	G_{IC}	ΔG_{IC}	$0.4 \times \Delta G_{IC}$	G_{IC}	ΔG_{IC}
Unmodified	101 ± 8	–	–	193 ± 12	–
3	313 ± 39	+212	+84	202 ± 13	+9
6	485 ± 35	+384	+153	173 ± 12	−20
9	762 ± 27	+661	+264	261 ± 24	+68
12	1112 ± 47	+1011	+404	296 ± 26	+103

3.5. Fractography

Scanning electron microscopy (SEM) was used to observe the fracture surfaces of the bulk epoxy polymers and syntactic foams. Images were taken in the plastic zone after the pre-crack to determine the toughening mechanisms. Note that the direction of crack propagation in all the images is from left to right.

3.5.1. Bulk epoxy polymer

The SEM images of the fracture surfaces of the CTBN modified bulk epoxy polymers are shown in Fig. 11. The fracture surfaces of the CTBN rubber modified epoxies are rougher than those of the unmodified epoxy. Micron-sized circular cavities can be observed, indicating that internal cavitation of the rubber particles has occurred. Some cavities are shallow and are lined with CTBN, while the deeper cavities show more obvious signs of rubber particle cavitation and subsequent plastic void growth, which can be seen as holes in the fracture surface. At higher CTBN concentrations, the deep cavities appear to become more sporadic, especially for the 12 wt% CTBN modified epoxy, as discussed below.

The diameters of the voids in the SEM micrographs were measured and compared to the particle sizes measured from the AFM micrographs. The distribution of the void radius also follows a log-normal distribution like the particle radius. The probability distribution functions of the void radius for 3 and 6 wt% CTBN modified epoxies are very similar, as shown in Fig. 12.

The mean radius of the cavities for the 3 and 6 wt% CTBN modified epoxies is 1.2 μm and the mode is 0.95 μm. It is clear that the radius of the cavities is larger than the radius of the particles, which have a mean radius of 0.87 μm and a mode radius of 0.63 μm. This shows that plastic void growth of the epoxy has occurred after cavitation of the CTBN particles. Cavitation of the rubber particles relieves the triaxial stress state ahead of the crack tip, allowing plastic void growth

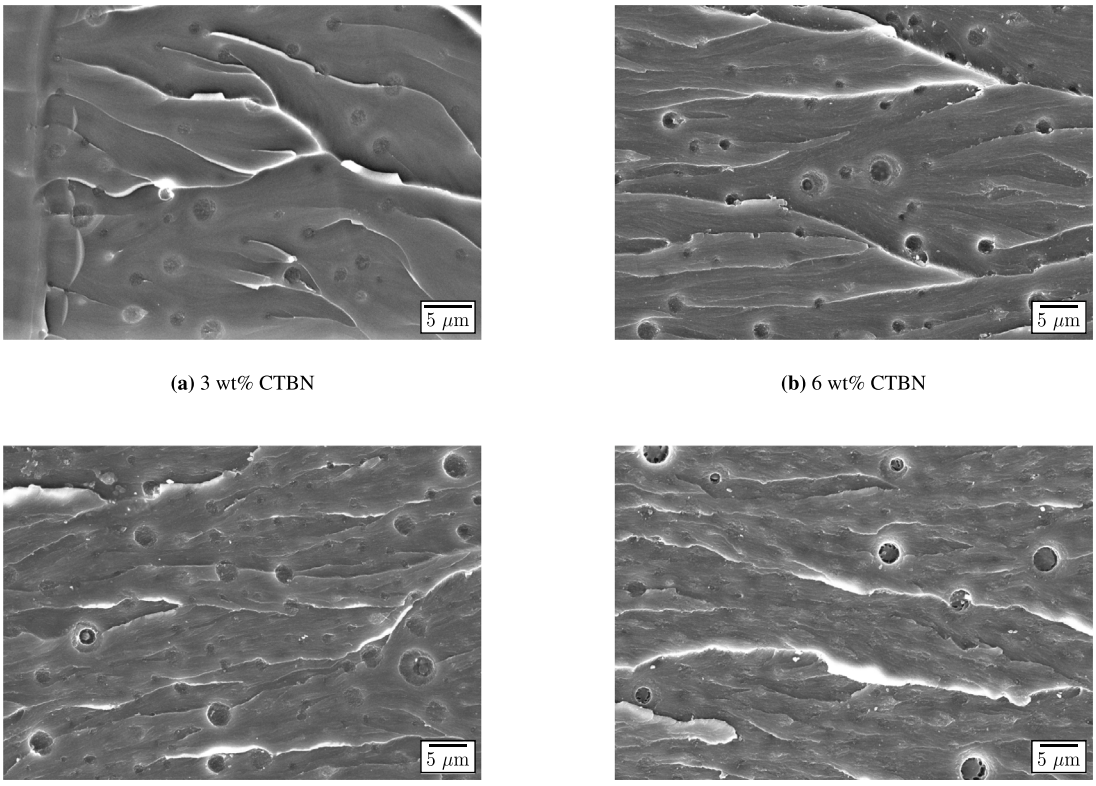

(a) 3 wt% CTBN **(b)** 6 wt% CTBN

(c) 9 wt% CTBN **(d)** 12 wt% CTBN

Fig. 11. Scanning electron micrographs of the fracture surfaces of CTBN rubber modified bulk epoxy polymers. Crack propagation direction is from left to right.

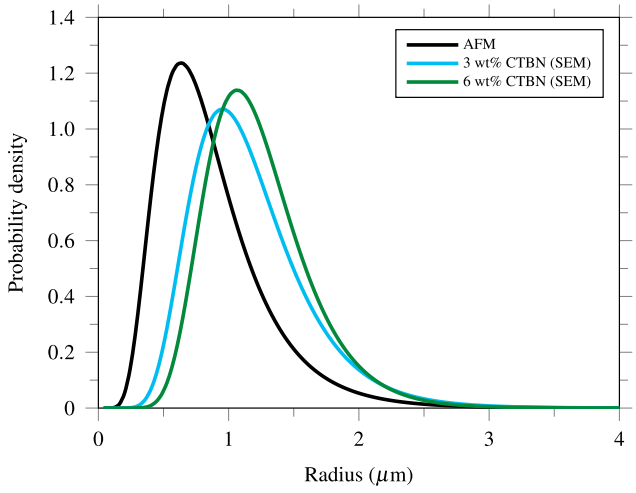

Fig. 12. Probability density distribution of particle radius from AFM and void radius from SEM of the fracture surfaces for 3 and 6 wt% CTBN.

of the epoxy to occur which absorbs a significant amount of energy and thus increases the fracture energy [30]. Thus, the plastic void growth toughening mechanism has been identified in this study.

When measuring the cavity sizes for the 9 wt% CTBN modified epoxy sample, an interesting distribution was observed where the void radius appears to follow a bimodal distribution. This supports the observation of the sporadic appearance of holes in the fracture surface at the higher CTBN concentrations, where the difference between shallow and deep cavities are more distinct. This bimodal distribution can be deconvoluted into two components, see Fig. 13. The probability distribution for the particle radius from the AFM micrographs is shown for comparison. It is clear that the distribution curve for the voids has split into two components from the original AFM curve. The shape of the first component is very similar to the original curve, indicating that not all of the particles exhibited plastic void growth after cavitation. This heavily implies that the second component represents the particles that did undergo plastic void growth. The proportions of the first and second components to the curve are 0.55 and 0.45, respectively, suggesting that only 45% of the CTBN rubber particles exhibited void growth. The modal value for void radius from the second component is also larger than those for the 3 and 6 wt% CTBN modified epoxies, of 1.42 μm. Since the diameters of the cavities in the SEM micrographs for the 12 wt% CTBN modified epoxy became difficult to measure and the voids also appear sporadic, bimodal behaviour is also assumed for this formulation. This information will be used in the modelling of fracture energy in Section 3.6.

An explanation for the transition in void growth behaviour can be found in terms of inter-particle spacing. Bray et al. [68] studied the effect of the debonding of silica nanoparticles from the surrounding matrix on the local stress field, using finite element analysis. They showed that nanoparticles directly adjacent to a void require a significantly higher energy to debond than an isolated particle. Hence, they concluded that these particles are shielded from debonding by the presence of the void. The energy required to debond particles that are further away from the void also greatly diminishes, hence the ability to debond the particle is dependent on the inter-particle spacing, which directly results from the volume fraction of the particles. An analogous statement can be made in this study, where cavitated rubber particles are shielded from void growth due to nearby voids. This becomes more apparent at smaller inter-particle spacing, which is why the bimodal behaviour was only observed at higher CTBN concentrations. Shielding of void growth is also evident in other studies on rubber modified epoxies [37,49], where the efficiency of toughening was reduced at higher wt% of particles.

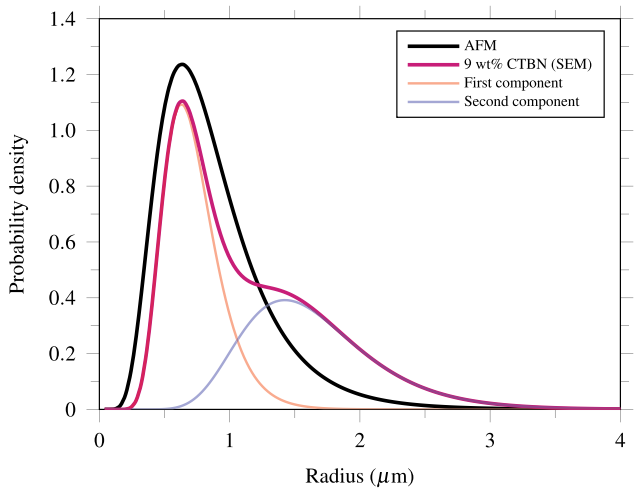

Fig. 13. Probability density distribution of particle radius from AFM and void radius from SEM for 9 wt% CTBN.

3.5.2. Syntactic foam

The fracture surfaces of the CTBN rubber modified syntactic foams were examined using SEM, and the images have been shown previously in Section 3.2.2 (Figs. 4 and 5). For the syntactic foams modified with 3 and 6 wt% CTBN, where the rubber particles displayed spherical morphology, no information is available on the initial size of the CTBN particles, since AFM was not possible on the syntactic foam samples. Whether plastic void growth of the epoxy matrix took place due to the cavitation of the rubber particles is therefore unclear. However, from the results of the SENB tests, no improvement in fracture energy compared to the unmodified foam was recorded for these formulations. From this, it can be inferred that no additional plastic deformation of the epoxy matrix has occurred due to the CTBN particles, as this would otherwise lead to an increase in fracture energy since it is a highly energy absorbent mechanism [30]. The reason for the lack of plastic void growth is due to the restricted space between the GMS particles. The ability for the epoxy to deform around the CTBN particles is therefore limited. Voids that are left by the debonding of GMS will also shield nearby rubber particles from undergoing void growth, as discussed above using the work by Bray et al. [68]. The size of the interstitial spaces can be increased by using lower volume fractions of GMS, however, this would come with an obvious penalty in density. Alternatively, using GMS particles with larger diameters can also be explored as this will increase the size of the interstitial spaces, allowing more plastic deformation.

The syntactic foams modified with 9 and 12 wt% CTBN showed co-continuous rubber morphologies, and these structures may be responsible for the increases in fracture energy observed in these formulations, see Table 3. Co-continuous structures have been found to cause large increases in fracture energy of block copolymer modified epoxies [41,69], although the toughening mechanisms and the modelling of fracture energy of co-continuous structures are not well understood. Chen and Taylor [41] proposed several mechanisms to explain the large improvements in toughness. In a co-continuous structure, the hard and soft composite-like structure spans across the fracture surface. The soft phase deforms and absorbs energy more readily than the epoxy phase, due to the low yield stress and high ductility of the soft phase. This deformation and energy absorption occurs before the epoxy ligaments spanning across the crack surfaces fracture, effectively blunting the crack tip and leading to large increases in fracture energy [42]. In addition, the connected structures can interact to greatly increase the size of the plastic deformation zone and thus increase toughness.

3.6. Modelling fracture energy

The major toughening mechanisms in this study of CTBN modified epoxies have been identified as shear band yielding and plastic void growth. The fracture energy contributions from these toughening mechanisms have been modelled by Huang and Kinloch [30,65], and the models are used here.

The fracture energy of the CTBN modified epoxies can be predicted analytically using the Huang and Kinloch model [30]:

$$G_{IC} = G_{ICU} + \Psi \tag{5}$$

where G_{ICU} is the fracture energy of the unmodified epoxy and Ψ is the sum of the fracture energy contributions from the identified toughening mechanisms. The latter can be written as:

$$\Psi = \Delta G_s + \Delta G_v \tag{6}$$

where ΔG_s and ΔG_v are the fracture energy contributions from shear band yielding and plastic void growth, respectively.

The fracture energy contribution from shear band yielding, ΔG_s, is given by [36]:

$$\Delta G_s = 0.5 V_p \sigma_{yc} \gamma_f F'(r_y) \tag{7}$$

where V_p is the volume fraction of particles present, σ_{yc} is the uniaxial compressive yield stress, and γ_f is the true fracture strain of the unmodified epoxy polymer. The uniaxial compressive yield stress can be determined from the plane strain compressive yield stress, σ_{psc}, using the following relationship derived from the Drucker–Prager yield criterion [30,40,70]:

$$\sigma_{yc} = \frac{3}{2}\sigma_{psc}\frac{\mu_m - 1}{\mu_m - \sqrt{3}} \tag{8}$$

where μ_m is the pressure dependent material constant. The value of μ_m was taken as 0.131 from a previous study [23]. The function $F'(r_y)$ is given by [36,71]:

$$F'(r_y) = r_y\left[\left(\frac{4\pi}{3V_p}\right)^{\frac{1}{3}}\left(1-\frac{r_p}{r_y}\right)^3 - \left(\frac{8}{5}\right)\left(1-\frac{r_p}{r_y}\right)\left(\frac{r_p}{r_y}\right)^{\frac{5}{2}} - \left(\frac{16}{35}\right)\left(\frac{r_p}{r_y}\right)^{\frac{7}{2}} - 2\left(1-\frac{r_p}{r_y}\right)^2 + \left(\frac{16}{35}\right)\right] \tag{9}$$

where r_p is the radius of the particle, and r_y is the radius of the plastic zone of the modified epoxy, which is defined as [30]:

$$r_y = K_{vm}^2\left(1+\frac{\mu_m}{\sqrt{3}}\right)^2 r_{yu} \tag{10}$$

where K_{vm} is the von Mises stress concentration factor, and r_{yu} is the radius of the plastic zone at fracture for the unmodified epoxy polymer under plane strain conditions. The value of K_{vm} depends on the particle volume fraction, and whether the particles are soft or rigid. For the case of CTBN rubber, they are classed as soft particles. The value of K_{vm} was calculated by fitting to the data of Huang and Kinloch [30]:

$$K_{vm} = 3.9337 V_p + 2.1126 \tag{11}$$

Huang and Kinloch applied a two-dimensional plane strain model to determine the values of K_{vm}, which has been shown to have better agreement with experimental observations in many cases than for the axisymmetric model proposed by Guild and Young [72]. The value of r_{yu} can be calculated using the equation proposed by Irwin [73]:

$$r_{yu} = \frac{1}{6\pi}\left(\frac{K_{ICU}^2}{\sigma_{yt}^2}\right) \tag{12}$$

where K_{ICU} and σ_{yt} are the fracture toughness and tensile yield stress of the unmodified epoxy, respectively. The value for σ_{yt} is taken as 88 MPa from a previous study using the same epoxy [23].

Table 4
Mechanical and fracture parameters of the unmodified bulk epoxy polymer, used in the modelling of fracture energy.

Parameter	Symbol	Unit	Value
Uniaxial tensile yield stress	σ_{yt}	MPa	88 ± 1 [23]
Plane strain compressive yield stress	σ_{psc}	MPa	122 ± 0.3
Uniaxial compressive yield stress	σ_{yc}	MPa	100
Compressive failure strain	γ_f	mm/mm	0.86 ± 0.01
Pressure dependent material constant	μ_m	–	0.131 [23]
Fracture energy	G_{ICU}	J/m^2	101 ± 8
Fracture toughness	K_{ICU}	MPa m$^{1/2}$	0.63 ± 0.03

Table 5
Parameters used in the modelling of fracture energy of CTBN modified epoxy polymers.

Parameter	Symbol	Unit	Value
Radius of CTBN particles	r_p	μm	Mean: 0.87 Mode: 0.63
Radius of voids	r_v	μm	Mean: 1.20[a] Mode: 0.95[a] Predicted: $(1+\gamma_f)r_p$
Volume fraction of CTBN particles	V_p	–	See Table 1

[a]For the 3 and 6 wt% CTBN modified bulk epoxy polymers only.

The plastic void growth contribution to the fracture energy, ΔG_v, can be calculated using [30]:

$$\Delta G_v = \left(1 - \frac{\mu_m^2}{3}\right)(V_v - V_p)\sigma_{yc} r_{yu} K_{vm}^2 \tag{13}$$

where V_v is the volume fraction of the voids, which may be measured directly from SEM micrographs, or a predictive method can be used. Assuming that the extent by which a void can grow is limited by the failure strain of the epoxy polymer, γ_f, then the circumferential strain of the void is equal to the failure strain, such that the radius of the void, r_v, can be predicted using:

$$r_v = (1 + \gamma_f) r_p \tag{14}$$

where r_p is the radius of the particle. The term $(V_v - V_p)$ can therefore be written as:

$$V_v - V_p = V_p\left[\left(1+\gamma_f\right)^3 - 1\right] \tag{15}$$

The value of Ψ can now be evaluated by combining Eqs. (7) and (13) to give:

$$\Psi = 0.5 V_p \sigma_{yc} \gamma_f F'(r_y) + \left(1 - \frac{\mu_m^2}{3}\right)(V_v - V_p)\sigma_{yc} r_{yu} K_{vm}^2 \tag{16}$$

The mechanical and fracture properties of the unmodified bulk epoxy polymer, which are used extensively in the above equations, are collated in Table 4 for convenience.

3.6.1. Bulk epoxy polymer

In the bulk epoxy polymer, the CTBN rubber phase separated into spherical particles. During the fracture process, these rubber particles cavitate and initiate shear band yielding and plastic void growth toughening mechanisms, which caused a significant increase in the fracture properties. The parameters of the spherical CTBN particles used in the modelling of these toughening mechanisms are shown in Table 5. The mean and modal values of the radius are listed, since the radii of the particles and the voids follow a log-normal distribution, see Fig. 12. Note that the radius values for the voids only apply for the bulk epoxy polymer modified with 3 and 6 wt% CTBN, since the voids follow a bimodal distribution at higher concentrations, see Fig. 13.

The fracture energy contributions from shear band yielding and void growth (for measured and predicted r_v values) can be calculated with the commonly used mean value approach, where the mean values for particle and void radii (see Table 5) are used, and are shown in Fig. 14(a). Adding these contributions to the fracture energy of the unmodified epoxy as per the Huang and Kinloch [30] model will give the analytical prediction for fracture energy for the bulk epoxy polymer, which is compared to the experimental results in Fig. 14(b). The analytical result which uses the measured mean value for void radius underestimates the fracture energy, while the analytical result which uses the predicted void radius overestimates the fracture energy.

The overestimation caused by using the predictive method for void radius is due to the assumption that all of the voids which initiated from cavitated rubber particles would grow until the failure strain of the epoxy is reached, which does not appear to be fully applicable for this study. This approach is truly predictive, meaning that fracture tests do not have to be performed and fracture surfaces analysed to perform the modelling. Previous work using nanoparticles, e.g. [31,43], has shown excellent agreement with experimental results, but when higher volume fractions or large (micron-sized) particles are used then the voids cannot grow to their full extent before failure and this approach overpredicts the toughening effect.

Using the mean value approach for the particle and void radii has been previously reported to underestimate the fracture energy in core–shell rubber modified epoxies [31], as also seen in this study, due to the fact that this approach does not take into account the underlying distribution of particle and void diameters. It can be argued that using the modal particle and void sizes (see Table 5) is more applicable, since those sizes are the most statistically probable. The result of using these modal values is that ΔG_s and ΔG_v are slightly increased, as shown in Fig. 15(a). Applying the Huang and Kinloch [30] model using the modal approach now shows excellent agreement with the experimental results for 3 and 6 wt% CTBN concentrations, see Fig. 15(b).

When the same modal particle and void radii are used for the 9 wt% and 12 wt% concentrations, the predictions agree less well with the experimental results due to the different size distributions at these concentrations (compare Figs. 12 and 13). Interpreting the bimodal distribution as discussed in Section 3.5.1, only 45% of the CTBN particles exhibited plastic void growth for these CTBN concentrations. The voids also grew to a larger size than for the 3 and 6 wt% CTBN modified epoxies, so the assumption that the voids grew to their full extent can be made. Therefore, the analytical model which uses the predicted void radius can be corrected by multiplying the toughening contribution from plastic void growth by a factor of 0.45. This value is an empirical factor that is obtained from the observation that 45% of the CTBN particles exhibited plastic void growth. The corrected prediction shows excellent agreement with the experimental results for 9 and 12 wt% CTBN concentrations, see Fig. 16. This highlights the importance of considering the underlying distribution of the particle and void sizes in the analytical modelling, from which the correction factor can be determined.

Note that the preceding modelling of the fracture energy considers the total volume fraction of CTBN rubber and therefore does not take into account the amount of CTBN rubber that remained dissolved in the epoxy polymer, which was evident by the decreased values for T_g at higher CTBN concentrations. This is common practice across studies on rubber modified epoxies, e.g. [31,36,43], as well as several types of block copolymer modified epoxies which also exhibit phase separation behaviour [42].

Since the equations for the fracture energy contributions from shear band yielding and plastic void growth depend on the volume fraction of the particles, V_p, it can be argued that the phase separated volume fraction should be used instead of the total volume fraction. This is because the volume fraction of particles should be analogous to the volume fraction that has phase separated. The modelling of the fracture energy was repeated using the phase separated volume fractions of CTBN, see Fig. 17. Comparison of the analytical and experimental values showed poor agreement at all CTBN concentrations except 3 wt%. This is due to the T_g of 3 wt% CTBN being the same as that of the unmodified

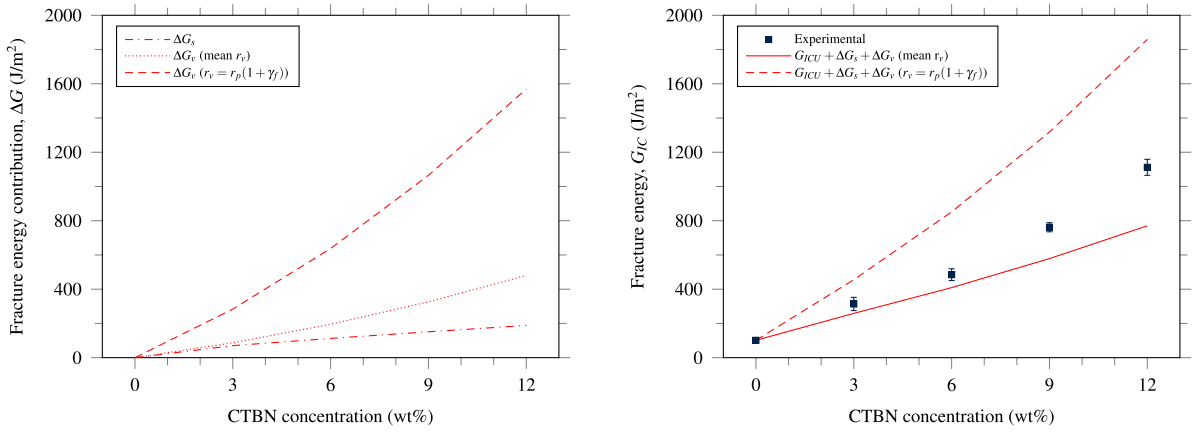

Fig. 14. **(a)** Fracture energy contributions for the shear band yielding and void growth toughening mechanisms, and **(b)** analytical and experimental fracture energy of CTBN modified epoxy polymers, using the mean value approach.

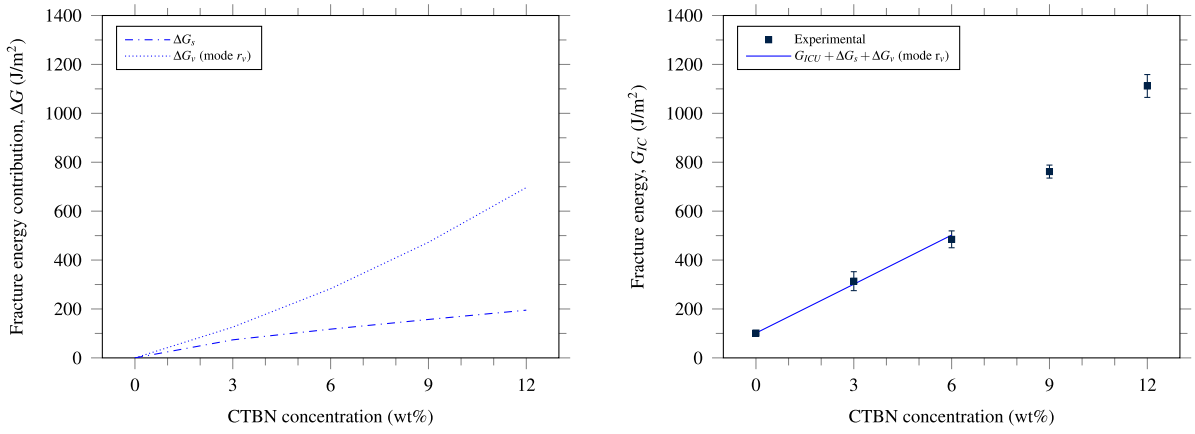

Fig. 15. **(a)** Fracture energy contributions for the shear band yielding and void growth toughening mechanisms and **(b)** analytical and experimental fracture energy of CTBN modified epoxy polymers, using the modal value approach.

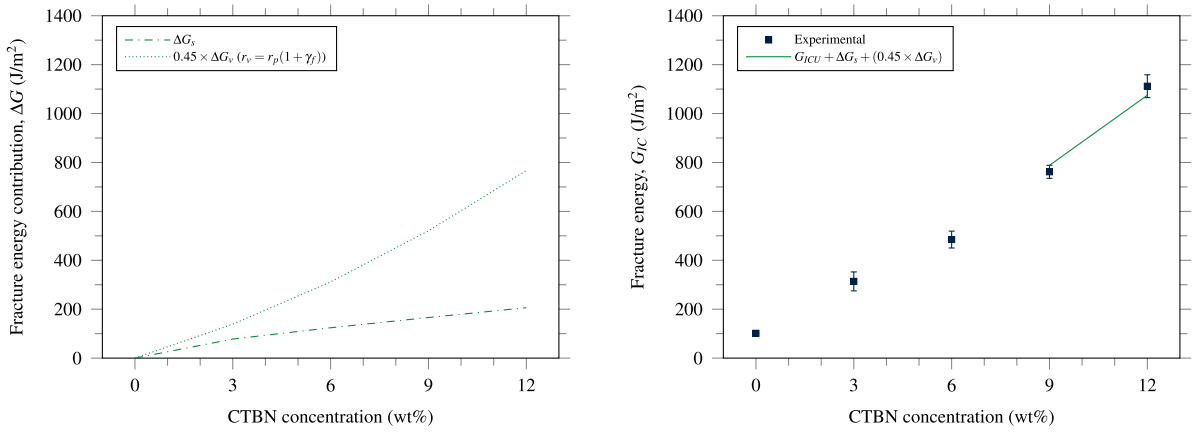

Fig. 16. **(a)** Fracture energy contributions for the shear band yielding and void growth toughening mechanisms and **(b)** analytical and experimental fracture energy of CTBN modified epoxy polymers, assuming that 45% of CTBN particles exhibited the full extent of plastic void growth as observed experimentally.

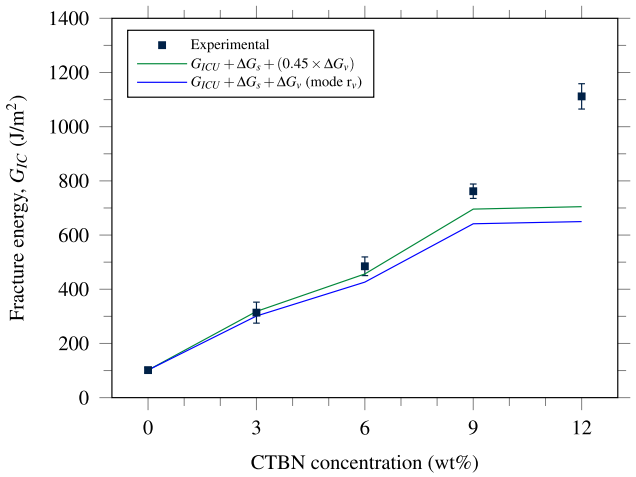

Fig. 17. Analytical and experimental fracture energy of CTBN modified epoxy polymers using phase separated CTBN volume fractions.

epoxy, which shows that the CTBN rubber has fully phase separated and therefore would not change the analytical result found previously. The result for 12 wt% CTBN showed particularly poor agreement since the drop in T_g at this concentration was relatively large.

The mechanical and fracture properties of the epoxy used in the modelling of the fracture energy are those of the unmodified epoxy polymer, see Table 5. The CTBN remaining dissolved in the epoxy resin will effectively plasticise the epoxy, reducing the modulus and yield stress, increasing strain to failure, and increasing the fracture toughness and energy. Using the mechanical properties of the epoxy with dissolved CTBN would therefore increase the predicted fracture energy, as can be seen by inspection of the equations in Section 3.6. However, samples of this epoxy cannot be manufactured for testing as the amount of CTBN which phase separates cannot be controlled. This means that using the phase separated CTBN volume fraction for the predictions is far less reliable at high CTBN contents, and therefore using the volume fraction of CTBN added gives the most reliable predictions of the fracture energy, as shown in Fig. 16.

3.6.2. Syntactic foam

Although spherical particle morphology was observed for the syntactic foams with 3 and 6 wt% CTBN, applying the Huang and Kinloch model as for the bulk epoxy polymers to syntactic foams would not agree with the experimental results, since no improvements in fracture energy were observed. Again this is due to the restricted space between the GMS particles. The deformation of the epoxy around the CTBN particles inside the syntactic foam is therefore limited. The debonding of the epoxy matrix from the GMS particles will also shield nearby rubber particles from undergoing plastic void growth, using the same explanation from Bray et al. [68] as discussed in Section 3.5.1. The redistribution of stress around the GMS particles after debonding will cause adjacent rubber particles to require much higher energies to undergo plastic void growth.

At higher CTBN concentrations, modelling the fracture energy of the syntactic foams is difficult, due to the complex rubber microstructures that phase separated within the spaces between the GMS particles at 9 and 12 wt% CTBN concentrations. Although the toughening mechanisms of co-continuous structures are discussed in Section 3.5.2, there are currently no models to predict the fracture energy contributions resulting from these mechanisms in the literature. It is proposed that the interconnected structures of rubber and epoxy can interact beyond the interstitial spaces between the hollow glass microspheres, effectively increasing the size of the plastic deformation zone. By inspection of Eq. (12), this explains the increases in fracture toughness.

4. Conclusions

The microstructure, fracture properties, and toughening mechanisms of bulk epoxy polymer and syntactic foam modified with CTBN were investigated and compared. For the bulk epoxy polymers, the CTBN phase separated into well-dispersed spherical particles for all CTBN concentrations. The CTBN also formed spherical particles in the syntactic foams at lower concentrations (3 and 6 wt%). As the concentration increases, the rubber particles begin to elongate along the surface of the GMS, forming co-continuous and phase inverted structures. The difference in CTBN morphology between the bulk epoxy polymer and syntactic foam was attributed to the reduced dimensionality coupled with particle coalescence in the growth evolution of phase separating CTBN rubber, introduced by the presence of the GMS.

The fracture energy showed a significant increase for the CTBN modified bulk epoxy polymers, from 101 ± 8 J/m^2 to 1112 ± 47 J/m^2 for 12 wt% CTBN. The toughening mechanisms were identified as shear band yielding and plastic void growth after cavitation of the rubber particles. Two methods in analytical modelling of these toughening mechanisms were used, a mean-value approach, and a statistical approach. The statistical approach showed excellent agreement to the experimental data, and performed much better than the conventional mean-value approach. This study has highlighted the importance of taking the underlying distribution of particle and void sizes into account during the modelling of fracture energy, which has often been neglected in the literature.

The fracture energy of the syntactic foams did not increase when the epoxy matrix was modified with 3 and 6 wt% CTBN and remained around 200 J/m^2, but increased gradually to 296 ± 26 J/m^2 at 12 wt%. The co-continuous structures that are present only at these high concentrations are thought to be the cause of the increase in toughness, due to the alternating hard–soft lamellar structure that spans across the fracture surface. However, this increase is much less than that achieved in the bulk epoxy polymer, therefore there is little transferability of toughness. Rubber particles in the syntactic foam have limited space in the interstitial regions between the GMS to undergo plastic void growth, so improvements in fracture energy are limited. Nevertheless, the toughness improvement achieved in this work allows for more lightweight, damage-resistant structures to be produced, increasing the number of applications of syntactic foams in the aerospace and naval industries.

CRediT authorship contribution statement

Sammy He: Conceptualization, Methodology, Investigation, Formal analysis, Writing – original draft, Writing – review & editing. **Declan Carolan:** Conceptualization, Methodology, Formal analysis, Writing – review & editing, Supervision. **Alexander Fergusson:** Conceptualization, Writing – review & editing, Supervision, Resources, Funding acquisition. **Ambrose C. Taylor:** Conceptualization, Writing – review & editing, Supervision, Resources, Funding acquisition.

Declaration of competing interest

The authors declare that they have no known competing financial interests or personal relationships that could have appeared to influence the work reported in this paper.

Data availability

Data will be made available on request.

Acknowledgements

This work was supported by an EPSRC Industrial CASE studentship funded by the UK Engineering and Physical Sciences Research Council and FAC Technology. Grant number: EP/N509486/1. Declan Carolan would like to acknowledge the support of UKRI Future Leaders Fellowship. Grant number: MR/T023406/1.

References

[1] Bunn P, Mottram JT. Manufacture and compression properties of syntactic foams. Composites 1993;24(7):565–71.
[2] Carolan D, Mayall A, Dear JP, Fergusson AD. Micromechanical modelling of syntactic foam. Composites B 2020;183:107701.
[3] Hobaica EC, Cook SD. The characteristics of syntactic foams used for buoyancy. J Cell Plast 1968;4(4):143–8.
[4] Gupta N, Zeltmann SE, Shunmugasamy VC, Pinisetty D. Applications of polymer matrix syntactic foams. JOM 2014;66(2):245–54.
[5] Gupta N, Woldesenbet E. Characterization of flexural properties of syntactic foam core sandwich composites and effect of density variation. J Compos Mater 2005;39(24):2197–212.
[6] Breunig P, Damodaran V, Shahapurkar K, Waddar S, Doddamani M, Jeyaraj P, Prabhakar P. Dynamic impact behavior of syntactic foam core sandwich composites. J Compos Mater 2020;54(4):535–47.
[7] Waddar S, Pitchaimani J, Doddamani M. Effect of thermal loading on syntactic foam sandwich composite. Polym Compos 2020;41(5):1774–84.
[8] Herrmann AS, Zahlen PC, Zuardy I. Sandwich structures technology in commercial aviation. In: Thomsen O, Bozhevolnaya E, Lyckegaard A, editors. Sandwich structures 7: Advancing with sandwich structures and materials. Dordrecht, The Netherlands: Springer; 2005, p. 13–26.
[9] Mouritz AP, Gellert E, Burchill P, Challis K. Review of advanced composite structures for naval ships and submarines. Compos Struct 2001;53(1):21–42.
[10] Aerospace Technology Institute. INSIGHT 09. Composite material applications in aerospace. Cranfield, UK: Aerospace Technology Institute; 2018.
[11] Gupta N, Woldensenbet E, Kishore . Compressive fracture features of syntactic foams-microscopic examination. J Mater Sci 2002;37:3199–209.
[12] Wouterson EM, Boey FYC, Hu X, Wong S. Specific properties and fracture toughness of syntactic foam: Effect of foam microstructures. Compos Sci Technol 2005;65(11–12):1840–50.
[13] Porfiri M, Gupta N. Effect of volume fraction and wall thickness on the elastic propertiesof hollow particle filled composites. Composites B 2009;40(2):166–73.
[14] Yousaf Z, Smith M, Potluri P, Parnell W. Compression properties of polymeric syntactic foam composites under cyclic loading. Composites B 2020;186:107764.
[15] Gupta N, Woldesenbet E. Microballoon wall thickness effects on properties of syntactic foams. J Cell Plast 2004;40(6):461–80.
[16] Huang R, Li P. Elastic behaviour and failure mechanism in epoxy syntactic foams: The effect of glass microballoon volume fractions. Composites B 2015;78:401–8.
[17] Wouterson EM, Boey FYC, Wong S-C, Chen L, Hu X. Nano-toughening versus micro-toughening of polymer syntactic foams. Compos Sci Technol 2007;67(14):2924–33.
[18] Asif A, Lakshmana Rao V, Ninan KN. Nanoclay reinforced thermoplastic toughened epoxy hybrid syntactic foam: Surface morphology, mechanical and thermo mechanical properties. Mater Sci Eng A 2010;572:6184–92.
[19] Zegeye E, Ghamsari AK, Woldesenbet E. Mechanical properties of graphene platelets reinforced syntactic foams. Composites B 2014;60:268–73.
[20] Ciardiello R, Drzal LT, Belingardi G. Effects of carbon black and graphene nanoplatelet fillers on the mechanical properties of syntactic foam. Compos Struct 2017;178:9–19.
[21] Zhang L, Ma J. Effect of carbon nanofiber reinforcement on mechanical properties of syntactic foam. Mater Sci Eng A 2013;574:191–6.
[22] Dando KR, Salem DR. The effect of nano-additive reinforcements on thermoplastic microballoon epoxy syntactic foam mechanical properties. J Compos Mater 2018;52(7):971–80.
[23] He S, Carolan D, Fergusson A, Taylor AC. Toughening epoxy syntactic foams with milled carbon fibres: Mechanical properties and toughening mechanisms. Mater Des 2019;169:107654.
[24] Wouterson EM, Boey FYC, Hu X, Wong S. Effect of fiber reinforcement on the tensile, fracture and thermal properties of syntactic foam. Polymer 2007;48(11):3183–91.
[25] Huang C, Huang Z, Qin Y, Ding J, Lv X. Mechanical and dynamic mechanical properties of epoxy syntactic foams reinforced by short carbon fiber. Polym Compos 2016;37(7):1960–70.
[26] Sultan JN, McGarry FJ. Effect of rubber particle size on deformation mechanisms in glassy epoxy. Fatigue Fract Eng Mater Struct 1973;13(1):29–34.
[27] Cahn JW, Hilliard JE. Free energy of a nonuniform system, I. Interfacial free energy. J Chem Phys 1958;28(2):258–67.
[28] Carolan D, Chong HM, Ivankovic A, Kinloch AJ, Taylor AC. Co-continuous polymer systems: A numerical investigation. Comput Mater Sci 2015;98:24–33.
[29] Bagheri R, Marouf BT, Pearson RA. Rubber-toughened epoxies: A critical review. J Macromol Sci C: Polym Rev 2009;49(3):201–25.
[30] Huang Y, Kinloch AJ. Modelling of the toughening mechanisms in rubber-modified epoxy polymers - Part II. A quantitative description of the microstructure-fracture property relationships. J Mater Sci 1992;27(10):2763–9.
[31] Carolan D, Ivankovic A, Kinloch AJ, Sprenger S, Taylor AC. Toughening of epoxy-based hybrid nanocomposites. Polymer 2016;97:179–90.
[32] Evonik . Technical data sheet Albipox 1000. Germany: Evonik; 2014.
[33] Huntsman Advanced Materials. Technical data sheet of Araldite LY 556 / Aradur HY 917 / Accelerator DY 070. Switzerland: Huntsman Corporation; 2007.
[34] Giannakopoulos G, Masania K, Taylor AC. Toughening of epoxy using core–shell particles. J Mater Sci 2011;46:327–38.
[35] Kunz SC, Sayre JA, Assink RA. Morphology and toughness characterization of epoxy resins modified with amine and carboxyl terminated rubbers. Polymer 1982;23(13):1897–906.
[36] Hsieh T-H, Kinloch AJ, Masania K, Sohn Lee J, Taylor AC, Sprenger S. The toughness of epoxy polymers and fibre composites modified with rubber microparticles and silica nanoparticles. J Mater Sci 2010;45(5):1193–210.
[37] Kunz SC, Beaumont PWR. Low-temperature behaviour of epoxy-rubber particulate composites. J Mater Sci 1981;16(11):3141–52.
[38] 3M. Technical data sheet of 3M glass bubbles S38. USA: 3M; 2010.
[39] ASTM D5418-15. Standard test method for plastics: dynamic mechanical properties: in flexure (dual cantilever beam). West Conshohocken, USA: American Society for Testing and Materials; 2015.
[40] Williams JG, Ford H. Stress–strain relationships for some unreinforced plastics. J Mech Eng Sci 1964;6(4):405–17.
[41] Chen J, Taylor AC. Epoxy modified with triblock copolymers: morphology, mechanical properties and fracture mechanisms. J Mater Sci 2012;47(11):4546–60.
[42] Chong HM, Taylor AC. The microstructure and fracture performance of styrene-butadiene-methylmethacrylate block copolymer-modified epoxy polymers. J Mater Sci 2013;48(19):6762–77.
[43] Keller A, Chong HM, Taylor AC, Dransfield C, Masania K. Core–shell rubber nanoparticle reinforcement and processing of high toughness fast-curing epoxy composites. Compos Sci Technol 2017;147:78–88.
[44] ISO 13586. Plastics - Determination of fracture toughness (G_{IC} and K_{IC}) - Linear elastic fracture mechanics (LEFM) approach. Geneva, Switzerland: International Organization for Standardization; 2018.
[45] Kinloch AJ, Shaw SJ, Tod DA, Houston DL. Deformation and fracture behaviour of a rubber-toughened epoxy: 1. Microstructure and fracture studies. Polymer 1983;24(10):1341–54.
[46] Wise CW, Cook WD, Goodwin AA. CTBN rubber phase precipitation in model epoxy resins. Polymer 2000;41(12):4625–33.
[47] Awang Ngah S, Taylor AC. Fracture behaviour of rubber- and silica nanoparticle-toughened glass fibre composites under static and fatigue loading. Composites A 2018;109:239–56.
[48] Fox TG. Influence of diluent and copolymer composition on the glass temperature of a polymer system. Bull Amer Phys Soc 1956;1(3):123.
[49] Kinloch AJ, Hunston DL. Effect of volume fraction of dispersed rubbery phase on the toughness of rubber-toughened epoxy polymers. J Mater Sci Lett 1987;6(2):137–9.
[50] Underwood EE. Quantitative stereology. Reading, USA: Addison-Wesley Pub. Co; 1970.
[51] Kiss LB, Söderlund J, Niklasson GA, Granqvist CG. New approach to the origin of lognormal size distributions of nanoparticles. Nanotechnology 1999;10(1):25–8.
[52] Yamanaka K, Inoue T. Phase separation mechanism of rubber-modified epoxy. J Mater Sci 1990;25(1):241–5.
[53] Chen J-P, Lee Y-D. A real-time study of the phase-separation process during polymerization of rubber-modified epoxy. Polymer 1995;36(1):55–65.
[54] McEwan I, Pethrick RA, Shaw SJ. Water absorption in a rubber-modified epoxy resin; carboxy terminated butadiene acrylonitrile-amine cured epoxy resin system. Polymer 1999;40(15):4213–22.
[55] Tripathi G, Srivastave D. Effect of carboxyl-terminated poly(butadiene-co-acrylonitrile) (CTBN) concentration on thermal and mechanical properties of binary blends of diglycidyl ether of bisphenol-A (DGEBA) epoxy resin. Mater Sci Eng A 2007;443(1–2):262–9.
[56] Wiltzius P, Cumming A. Domain growth and wetting in polymer mixtures. Phys Rev Lett 1991;66(23):3000–3.
[57] Cumming A, Wiltzius P, Bates FS, Rosedale JH. Light-scattering experiments on phase-separation dynamics in binary fluid mixtures. Phys Rev A 1992;45(2):885–97.
[58] Hair ML. Hydroxyl groups on silica surface. J Non-Cryst Solids 1975;19:299–309.
[59] Andrews EH, Pingsheng He, Vlachos C. Adhesion of epoxy resin to glass. Proc R Soc Lond A 1982;381(1781):345–60.
[60] Troian SM. Coalescence induced domain growth near a wall during spinodal decomposition. Phys Rev Lett 1993;71(9):1399–402.
[61] Torres FE, Troian SM. Diffusive growth of phase-separating domains near a surface: the effect of reduced dimensionality. Colloids Surf 1994;89(2–3):227–39.
[62] Rogers TM, Elder KR, Desai RC. Droplet grwoth and coarsening during heterogeneous vapor condensation. Phys Rev A 1988;38(10):5303–9.
[63] Bowden PB. The yield behavior of glassy polymers. In: Haward RN, editor. The physics of glassy polymers. London, UK: Applied Science Publishers Ltd; 1973.
[64] Pearson RA, Yee AF. Toughening mechanisms in elastomer-modifed epoxies - Part 2. Microscopy studies. J Mater Sci 1986;21:2475–88.
[65] Huang Y, Kinloch AJ. Modelling of the toughening mechanisms in rubber-modified epoxy polymers - Part I. Finite element analysis studies. J Mater Sci 1992;27(10):2753–62.
[66] Yee AF, Li D, Li X. The importance of constraint relief caused by rubber cavitation in the toughening of epoxy. J Mater Sci 1993;28:6392–8.

[67] Gent AN. Detachment of an elastic matrix from a rigid spherical inclusion. J Mater Sci 1980;15(11):2884–8.
[68] Bray DJ, Dittanet P, Guild FJ, Kinloch AJ, Masania K, Pearson RA, Taylor AC. The modelling of the toughening of epoxy polymers via silica nanoparticles: The effects of volume fraction and particle size. Polymer 2013;54(26):7022–32.
[69] Klinger A, Bajpai A, Wetzel B. The effect of block copolymer and core–shell rubber hybrid toughening on morphology and fracture of epoxy-based fibre reinforced composites. Eng Fract Mech 2018;203:81–101.
[70] Drucker DC, Prager W. Soil mechanics and plastic analysis or limit design. Quart Appl Math 1952;10(2):157–65.
[71] Hsieh T-H, Kinloch AJ, Masania K, Sohn Lee J, Taylor AC, Sprenger S. Erratum to: The toughness of epoxy polymers and fibre composites modified with rubber microparticles and silica nanoparticles. J Mater Sci 2011;46(11):4092.
[72] Guild FJ, Young RJ. A predictive model for particulate-filled composite materials - Part 2. Soft particles. J Mater Sci 1989;24(7):2454–60.
[73] Irwin GR. Plastic zone near a crack and fracture toughness. In: Meeting of the 7th Sagamore Ordnance Materials Research Conference. Racquette Lake, USA; 1960, p. 63–78.